13th Australasian Fluid Mechanics Conference
Monash University, Melbourne, Australia
13-18 December 1998

FLOW DYNAMICS IN THE 'SLICED CONE' MODEL OF WIND-DRIVEN OCEAN CIRCULATION

Andrew E. KISS and Ross W. GRIFFITHS

Research School of Earth Sciences
Australian National University, Canberra, ACT, AUSTRALIA

ABSTRACT

The 'sliced cone' laboratory model was introduced by Griffiths and Veronis (1997) (hereafter, GV97) to investigate the effect of sloping sidewalls on homogeneous wind-driven flow on a β-plane. This model is a variant of the 'sliced cylinder' model of Pedlosky and Greenspan (1967) in which the vertical sidewalls have been replaced by an azimuthally uniform slope around the perimeter of the basin. This modification has the twin effects of closing the basin's geostrophic contours and of largely removing the lateral dissipation of vorticity at the boundaries, leaving Ekman friction as the dominant dissipation mechanism. The laboratory flows observed by GV97 showed a dramatic difference in stability depending on the sign of the simulated wind stress curl. Flows produced by anticyclonic forcing were unsteady even for very weak forcing, and displayed eddy-shedding instabilities under stronger forcing. In contrast, the flow driven by cyclonic forcing was stable and steady under all conditions investigated.

This paper presents results of a numerical study of this system, which clarifies the dynamics of the observed flows and offers an explanation for the dependence of stability on the sign of the wind stress curl.

INTRODUCTION

Recent analytical and numerical results by Salmon (1992) and Becker and Salmon (1997) have shown that the barotropic flow in simple β-plane models of wind-driven ocean circulation is dramatically altered when the vertical boundaries usually employed in such models are replaced by continental slopes on which the depth goes gradually to zero at the boundaries. The sloping topography acts to guide the barotropic flow and moves the western boundary currents away from the lateral boundaries and onto the lower part of the slope. This produces a vorticity distribution which is more prone to instabilities than in the case of vertical sidewalls and diminishes the role of lateral viscosity at the boundary in dissipating potential vorticity.

A similar geometry (the 'sliced cone' - see Figure 1) was investigated in the laboratory by GV97 and a linear analysis based on an expansion in powers of $E^{\frac{1}{2}}$ was presented by Griffiths and Veronis (1998) (hereafter, GV98). This analysis showed that the zeroth order flow is along geostrophic contours, and is therefore about ten times faster on the slope than in the interior due to the order of magnitude difference of the bottom slopes in these regions. The $E^{\frac{1}{2}}$-order correction introduces the effect of wind forcing in the interior, resulting in a cross-contour Sverdrup flow which gives a northwest-southeast tilt to the streamlines in the interior but relatively little change to the slope current. At the next order a Stewartson $E^{\frac{1}{4}}$ layer at the junction between the rapid slope current and the slow interior flow makes the azimuthal velocity continuous in this region. The presence of closed geostrophic contours provides a "short cut" for the western boundary current of the interior Sverdrup flow, allowing the current to delay dissipation of the potential vorticity imparted by the wind until just before it rejoins the interior flow.

This paper presents an analysis of several numerical simulations of the flow in this apparatus.

THE 'SLICED CONE' MODEL

The laboratory model employed by GV97 utilised a basin of the form shown in Figure 1, filled with water and bounded above by a rigid horizontal lid. The base of the apparatus rotates with a constant angular velocity $\Omega\hat{\mathbf{k}}$ about a vertical axis, whilst the rigid lid has a slightly different angular velocity $(1+\epsilon)\,\Omega\hat{\mathbf{k}}$ in order to simulate a spatially uniform wind stress curl. The sidewall has a 45° slope relative to the horizontal and this cone is intersected by a plane with slope 1:10 which forms the central part of the bottom boundary. Figure 1 shows that in this geometry the geostrophic contours (contours of constant depth) are circles near the rim and D-shaped curves when they cross the interior. All geostrophic contours are closed curves, in contrast to the 'sliced cylinder' in which all geostrophic contours are blocked by the vertical sidewalls. The potential vorticity gradient imposed by the shallow slope in the interior is analogous to the

potential vorticity gradient of a β-plane and allows us to identify directions in the apparatus with various points of the compass, as shown in the figure (note that the apparatus rotates in the northern hemisphere sense). The width $2a$ of the apparatus is 0.973 m and the depth H at the centre is 0.125 m.

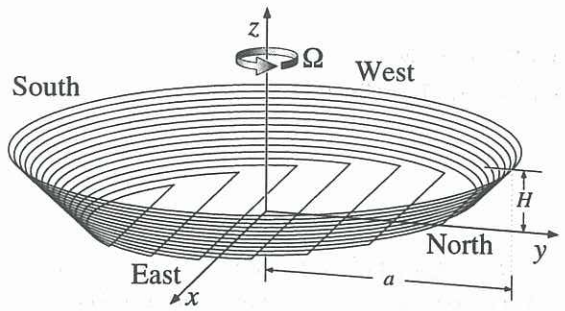

Figure 1: Perspective diagram of the 'sliced cone' model used in the laboratory and numerical experiments. The curves are contours of constant depth (geostrophic contours).

Formulation

The equations of motion for this system (relative to coordinates rotating with angular velocity $\Omega\hat{\mathbf{k}}$) are:

$$\frac{\partial \mathbf{u}}{\partial t} + Ro\,(\mathbf{u}\cdot\nabla)\,\mathbf{u} + 2\hat{\mathbf{k}}\times\mathbf{u} = -\nabla p + E\nabla^2\mathbf{u} \tag{1}$$

and

$$\nabla\cdot\mathbf{u} = 0, \tag{2}$$

where $\hat{\mathbf{k}}$ is the unit vector in the z direction (vertical), p is the pressure divided by the density and we have scaled the velocity $\mathbf{u}$, time t and length by $|\epsilon\Omega H|$, $|\Omega^{-1}|$ and H, respectively. With this scaling the importance of advection and viscosity are parameterised by the Rossby number $Ro = |\epsilon|$ and Ekman number $E = \frac{\nu}{\Omega H^2}$, respectively, where ν is the kinematic viscosity of the fluid.

We shall separate the vertical and horizontal components of the velocity by writing $\mathbf{u} = \mathbf{u}_H + \hat{\mathbf{k}}w$, where $\hat{\mathbf{k}}\cdot\mathbf{u}_H = 0$. For the parameters used in this study it is a very good approximation to assume (outside the Ekman layers) that $\mathbf{u}_H$ is independent of z and horizontally nondivergent, so we have

$$\mathbf{u}_H = \hat{\mathbf{k}}\times\nabla_H\psi, \tag{3}$$

where ψ is the streamfunction and ∇_H denotes the horizontal gradient operator.

Taking the vertical component of the curl of the momentum equation (1) yields an equation for the vertical vorticity ζ:

$$\frac{\partial\zeta}{\partial t} + RoJ(\psi,\zeta) = (2+Ro\zeta)\frac{\partial w}{\partial z} + E\nabla_H^2\zeta, \tag{4}$$

where

$$\zeta = \nabla_H^2\psi \tag{5}$$

and $J(a,b) \equiv \frac{\partial a}{\partial x}\frac{\partial b}{\partial y} - \frac{\partial a}{\partial y}\frac{\partial b}{\partial x}$ is the two-dimensional Jacobian operator. The assumption that $\frac{\partial \mathbf{u}_H}{\partial z} = \mathbf{0}$ implies (via (2)) that $\frac{\partial^2 w}{\partial z^2} = 0$, allowing us to find $\frac{\partial w}{\partial z}$ by using steady, linear Ekman matching conditions to find w at the top and bottom boundaries. On the slope this yields

$$\begin{aligned} 2\,(1-h)\,\frac{\partial w}{\partial z} =& E^{\frac{1}{2}}\,(\zeta_T - (1+\sigma)\,\zeta) \\ & - E^{\frac{1}{2}}s^2\sigma\frac{\partial^2\psi}{r^2\partial\theta^2} \\ & - 2J(\psi,h)\,, \end{aligned} \tag{6}$$

where $\zeta_T = 2\frac{\epsilon}{|\epsilon|}$ is the vorticity of the lid, $1-h$ is the scaled fluid depth, $s = |\nabla_H h|$ is the bottom slope, $\sigma = \left(1+s^2\right)^{\frac{1}{4}}$, and r and θ are the radial and azimuthal coordinates. This expression for $\frac{\partial w}{\partial z}$ includes the modification to the bottom Ekman layer due to the slope, as derived by Pedlosky (1987). In the interior the bottom slope is so small that its effect on the bottom Ekman layer can be neglected, giving

$$\begin{aligned} 2\,(1-h)\,\frac{\partial w}{\partial z} =& E^{\frac{1}{2}}\,(\zeta_T - 2\zeta) \\ & - 2J(\psi,h)\,. \end{aligned} \tag{7}$$

The no-slip boundary condition gives

$$\psi = \frac{\partial\psi}{\partial r} = 0 \qquad \text{at } r = \frac{a}{H}. \tag{8}$$

The numerical model

The numerical experiments were conducted with a highly efficient sliced-cylinder code developed by Page (1982) and described in detail in his PhD thesis (Page, 1981). For this study the code was modified to include the effect of the sloping sidewalls on the bottom Ekman layer. The code solves (4) and (5), where $\frac{\partial w}{\partial z}$ is found by using (6) on the slope[1] and (7) in the interior. This system generalises that analysed by GV98 by including advection, lateral viscosity and time dependence. Spatial derivatives are calculated using second-order centred differences on a polar grid, except at the origin where a special integral treatment is used. The vorticity equation (4) is advanced in time using the alternating-direction implicit method, and a fast Fourier transform in θ is used to solve the Poisson equation (5) for ψ. Since the nonlinearity in (4) couples it to (5), these equations are solved iteratively within each timestep until both ψ and ζ converge. This in-timestep iteration also serves to converge ζ at the boundary to a value which is consistent with

[1] (6) is not evaluated on the boundary itself (where $\frac{\partial w}{\partial z}$ diverges) because this is where (8) is imposed

the no-slip boundary condition (8). The algorithm is unconditionally stable for zero Ro and retains its stability for all reasonable values of Ro. The numerical results reported here were obtained using 160 grid points in the radial direction and 512 in the azimuthal direction (with no stretching in either direction) and a timestep of $10^{-3}E^{-\frac{1}{2}}$ rotation periods.

RESULTS

The numerical results presented here duplicate some of the laboratory experiments performed by GV97, and serve both to validate the numerical method used and to shed light on the vorticity dynamics of these flows. Following GV97, the simulations were performed with a fixed value of $E = 3.15 \times 10^{-5}$, with both anticyclonic and cyclonic forcing of various magnitudes (ie various Ro). The numerical simulations were spun-up from rest and run for 4000 timesteps (about 710 rotation periods for $E = 3.15 \times 10^{-5}$).

Anticyclonic forcing

Streamfunction and vorticity contours under anticyclonic forcing are shown in Figure 2. The flow is relatively rapid on the slope and much weaker in the interior, resulting in a region of strong anticyclonic vorticity at the bottom of the slope. The flows with $Ro = 0.43 \times 10^{-2}$ or 1.51×10^{-2} are steady, whereas the flow with $Ro = 5.2 \times 10^{-2}$ is unstable, displaying anticyclonic eddy shedding from the breakup of the anticyclonic gyre and cyclonic eddy shedding from a cyclonic meander of the western boundary current jet where it penetrates into the interior. Figure 3 shows a sequence of snapshots of the flow with an intermediate Rossby number, where only anticyclonic eddy shedding is present. These numerical results are almost indistinguishable from those obtained in the laboratory under the same conditions.

Cyclonic forcing

Figure 4 shows streamfunction and vorticity contours of the flow under cyclonic forcing. In this case the region between the rapid slope current and the slow interior flow has cyclonic vorticity. The vorticity distribution for $Ro = 0.41 \times 10^{-2}$ is very similar (apart from sign) to the distribution with small Ro under anticyclonic forcing. For larger Ro there is a marked difference, the distribution under cyclonic forcing being much more uniform in the azimuthal direction. The flows are stable for all Rossby numbers investigated, even for Ro much larger than that required to produce instability under anticyclonic forcing. As in the anticyclonic forcing case, these numerical results closely match those seen in the laboratory.

DISCUSSION

Plots (not shown) of the dominant balance in the vorticity equation (4) in different regions have revealed

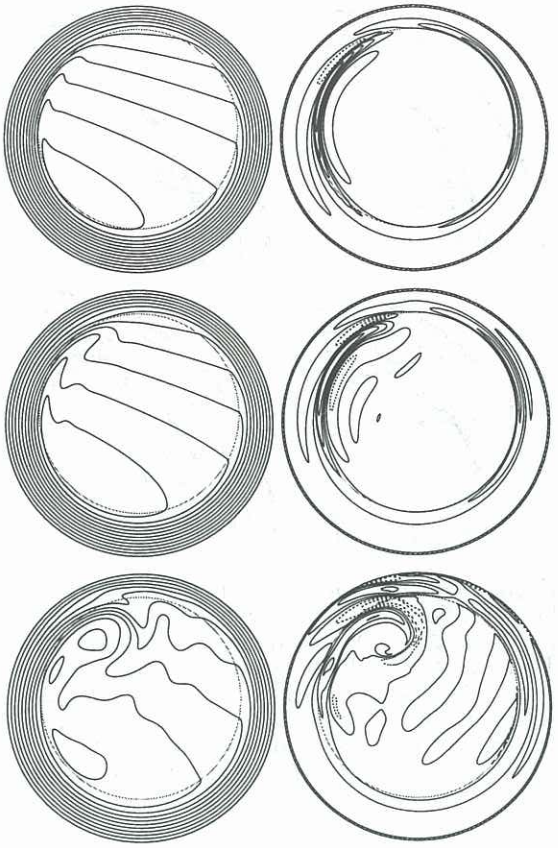

Figure 2: Contours of ψ (left) and ζ (right) under anticyclonic forcing with $E = 3.15 \times 10^{-5}$. Top: $Ro = 0.43 \times 10^{-2}$; middle: $Ro = 1.51 \times 10^{-2}$; bottom: $Ro = 5.2 \times 10^{-2}$. Contours of cyclonic ζ are dashed, and the grey line marks the bottom of the slope. Contour intervals for ψ and ζ are the same for all Rossby numbers, but note that ψ and ζ are scaled by Ro in the formulation.

that for small Ro the flow in the interior is controlled by a balance between wind forcing and cross-contour flow (equivalent to the Sverdrup balance in the oceans), and the flow on most of the slope is dominated by a balance between wind forcing and Ekman dissipation, with a smaller contribution from cross-contour flow. Between these regions the strong vorticity of the flow leads to a balance between Ekman dissipation and cross-contour flow. These results support the asymptotic analysis of GV98. In addition, these balances reduce (4) to $\frac{\partial w}{\partial z} \approx 0$, consistent with our assumption of horizontally nondivergent flow.

Advection of vorticity plays an increasingly important role in the vorticity balance as the Rossby number is increased, but the flows which result are dramatically different depending on the sign of the surface wind stress curl. Under anticyclonic forcing, increasing Ro tends to make the relative vorticity 'pile up' at the downstream end of the western boundary current (see Figure 2), eventually leading to instabilities in this region. In contrast, increasing Ro under cyclonic forcing results in a vorticity distribution which

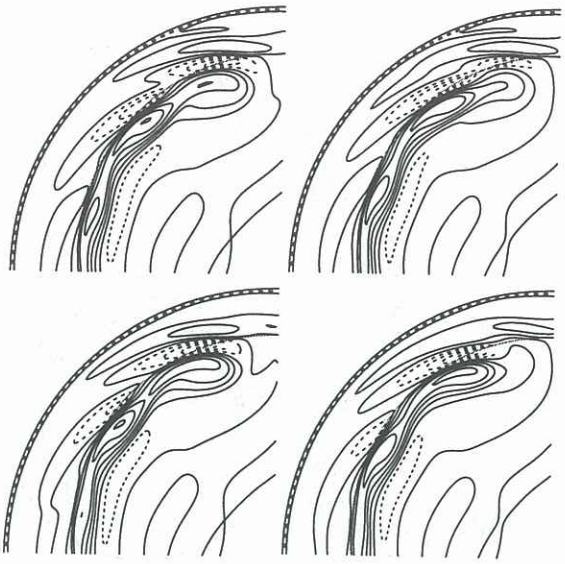

Figure 3: Sequence of vorticity contour plots for the flow under anticyclonic forcing with $E = 3.15 \times 10^{-5}$ and $Ro = 2.07 \times 10^{-2}$. These plots should be viewed in clockwise order. They were taken at intervals of $0.25T$, where T is the oscillation period (20.6 days). An animation of this sequence can be viewed at http://rses.anu.edu.au/gfd/link/AK/AFMC13.html

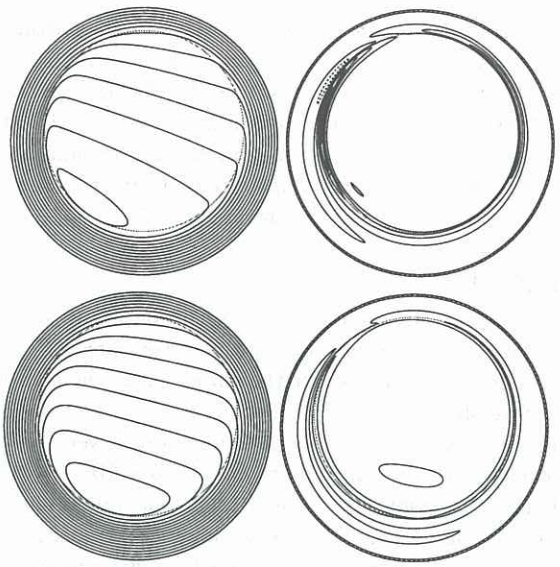

Figure 4: Contours of ψ (left) and ζ (right) under cyclonic forcing with $E = 3.15 \times 10^{-5}$. Top: $Ro = 0.41 \times 10^{-2}$; bottom: $Ro = 3.57 \times 10^{-2}$. Contours of anticyclonic ζ are dashed. The contour intervals are the same as in Figure 2.

is *more* homogeneous in the azimuthal direction, as shown in Figure 4. This difference may be related to the direction of the flow relative to the direction of phase propagation of linear topographic Rossby waves. These waves travel to the west in the interior and counterclockwise on the slope, which is in the same direction as the flow under cyclonic forcing but counter to the flow under anticyclonic forcing. As a result, linear standing waves are possible only under anticyclonic forcing, allowing the existence of isolated vorticity anomalies (for example, the vorticity balance in the meandering western boundary current jet indicates that this is an Ekman-damped standing Rossby wave). Under cyclonic forcing such dynamics are impossible and increased advection acts to homogenise the vorticity along the streamlines.

The breakdown of the anticyclonic gyre under strong anticyclonic forcing with small E can be understood in terms of the distribution of potential vorticity, $q = (2 + Ro\zeta)/(1 - h)$. When $\zeta = 0$, contours of q are geostrophic contours (see Figure 1): q is very large near the boundaries and decreases with increasing depth. Under anticyclonic forcing ζ is negative at the bottom of the sidewall, and this produces an extended 'tongue' of low potential vorticity along the western side of the interior, making the flow in this region susceptible to barotropic instability (see Figure 3). In contrast, under cyclonic forcing the cyclonic vorticity of the Stewartson layer increases q in this region, smoothing out the corners of the D-shaped region of low q in the deepest part of the interior and making baroclinic instability less likely.

The instability in the western boundary current jet which appears at larger Rossby numbers under anticyclonic forcing is the same as that seen in the sliced cylinder apparatus, and a kinematic argument given by GV97 explains why it is only seen under anticyclonic forcing. At larger E this is the only instability mechanism present.

REFERENCES

BECKER, J. M. AND SALMON, R., "Eddy formation on a continental slope", *J. Mar. Res.* **55**, 181–200, 1997.

GRIFFITHS, R. W. AND VERONIS, G., "A laboratory study of the effects of a sloping side boundary on wind-driven circulation in a homogeneous ocean model", *J. Mar. Res.* **55**, 1103–1126, 1997.

GRIFFITHS, R. W. AND VERONIS, G., "Linear theory of the effect of a sloping boundary on circulation in a homogeneous laboratory model", *J. Mar. Res.* **56**, 75–86, 1998.

PAGE, M. A., "Rotating fluids at low Rossby number", Phd thesis, University College, London, 1981.

PAGE, M. A., "A numerical study of detached shear layers in a rotating sliced cylinder", *Geophys. Astrophys. Fluid Dyn.* **22**, 51–69, 1982.

PEDLOSKY, J., *Geophysical fluid dynamics*, 2nd edn. New York: Springer, 1987.

PEDLOSKY, J. AND GREENSPAN, H. P., "A simple laboratory model for the oceanic circulation", *J. Fluid Mech.* **27**, 291–304, 1967.

SALMON, R., "A two-layer gulf stream over a continental slope", *J. Mar. Res.* **50**, 341–365, 1992.